aval Research Laboratory
shington, DC 20375-5320

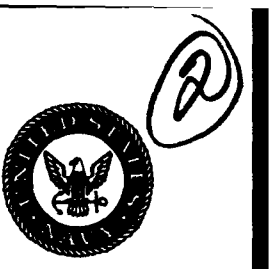

NRL/MR/6720--94-7428

Power Flow and PRS Optimization on Phoenix

ROBERT E. TERRY

Radiation Hydrodynamics Branch
Plasma Physics Division

FREDERICK L. COCHRAN

Berkeley Research Laboratory

March 28, 1994

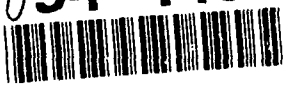

REPORT DOCUMENTATION PAGE

Form Approved
OMB No. 0704-0188

1. AGENCY USE ONLY (*Leave Blank*)	2. REPORT DATE	3. REPORT TYPE AND DATES COVERED
	March 28, 1994	

4. TITLE AND SUBTITLE

Power Flow and PRS Optimization on Phoenix

5. FUNDING NUMBERS

6. AUTHOR(S)

Robert E. Terry and Frederick L. Cochran*

7. PERFORMING ORGANIZATION NAME(S) AND ADDRESS(ES)

Naval Research Laboratory
Washington, DC 20375-5320

8. PERFORMING ORGANIZATION REPORT NUMBER

NRL/MR/6720--94-7428

9. SPONSORING/MONITORING AGENCY NAME(S) AND ADDRESS(ES)

Naval Surface Warfare Center
Dahlgren, VA 22448-5000

10. SPONSORING/MONITORING AGENCY REPORT NUMBER

11. SUPPLEMENTARY NOTES

*Berkeley Research Laboratory

12a. DISTRIBUTION/AVAILABILITY STATEMENT

Approved for public release; distribution unlimited.

12b. DISTRIBUTION CODE

13. ABSTRACT (*Maximum 200 words*)

The DNA Phoenix program has investigated (i) the power flow in the front end magnetically insulated transmission line (MITL) and PRS load assembly, to identify any losses, and model them, and (ii) the optimum injection angle and mass loading for a specific puff gas nozzle assembly. An optimum PRS mass loading can convert about 10-15% of the energy delivered to the front end into load kinetic energy over a range of 4.65 - 5.7 nH of initial PRS loading inductance. Specific kinetic energy per ion tends to fall off monotonically as the PRS length exceeds 4.5 cm. The gas puff optimization investigated nozzle designs which could optimize the uniformity of the implosion through high Mach number and tilting. The best yields for Argon were found at 12° for a Mach 4 nozzle, and 7.5° for a Mach 5 nozzle. The yield at the optimum tilt angle does not vary strongly with Mach number.

14. SUBJECT TERMS

Power flow
Gas puff nozzle

15. NUMBER OF PAGES

34

16. PRICE CODE

17. SECURITY CLASSIFICATION OF REPORT	18. SECURITY CLASSIFICATION OF THIS PAGE	19. SECURITY CLASSIFICATION OF ABSTRACT	20. LIMITATION OF ABSTRACT
UNCLASSIFIED	UNCLASSIFIED	UNCLASSIFIED	UL

NSN 7540-01-280-5500

Standard Form 298 (Rev. 2-89)
Prescribed by ANSI Std 239-18
298-102

CONTENTS

POWER FLOW AND PRS OPTIMIZATION ON PHOENIX

I. EXECUTIVE SUMMARY

As an element in the DNA program to upgrade Phoenix and to modernize its plasma radiation source (PRS) capability, the studies discussed here have served two general purposes. The first task was to describe the power flow in the front end magnetically insulated transmission line (MITL) and PRS load assembly, to identify any losses, and model them. The second task was to determine the optimum injection angle and mass loading for the SRL puff gas nozzle assembly. Regarding general power flow, we have found that an optimum PRS mass loading can convert about 10→15% of the energy delivered (past the waterline voltage monitor) to the front end into load kinetic energy over a range of 4.65 → 5.7 nH of initial PRS load inductance. Further, the azimuthally averaged monitor voltage can be roughly verified in its calibration through the modeling of "short circuit" load events. Once the insulator flashover is modeled, the PRS behavior is successfully described with only modest losses in the MITL due to magnetic insulation failure at load stagnation. Kinetic energy transfer is found to vary in a more regular way with inductance for longer PRS lengths, but specific kinetic energy per ion tends to fall off monotonically as the PRS length exceeds 4.5 cm.

The optimization of the gas puff load investigated nozzle designs which could optimize the uniformity of the implosion through high Mach number and tilting. The best yields for Argon were found at 12° for a Mach 3 nozzle, 9° for a Mach 4 nozzle, and 7.5° for a Mach 5 nozzle. The yield at the optimum tilt angle does not vary strongly with Mach number over the domain examined.

II. POWER FLOW

Phoenix comprises (i) a Marx bank, (ii) a pulse forming water line, (iii) a prepulse suppression switch, (iv) a second water transformer (terminated in a radial taper and vacuum insulator stack), (v) a constant impedance biconic output line, (vi) a variable impedance conical MITL, and (vii) a load chamber. For the purposes of PRS coupling, the existing set of voltage monitors in the water transformer serve to define an input

Manuscript approved January 11, 1994.

voltage boundary condition, and this constraint includes a general reflection of power from the load that begins about 100 ns after pulse initiation. A typical dataset will include a measure of the energy transferred downstream of the voltage and current monitors in the water line. The energy transfer that is inferred from this data is usually consistent with the computed energy transfer in the transmission line model.

Line Model Elements

The Phoenix model discussed here is an abbreviated one in that no attempt is made to describe all the power flow details upstream of the voltage monitors in the second water transformer. The voltage waveform inferred from the monitor (called Tube Voltage or TV below) is used as a temporal boundary condition on the transmission line model. Hence the current generated in the model line is the prime measure of the model's accuracy with respect to experimental current traces inferred from any downstream stations. All such voltage waveforms show that power flow always reverses during a shot, reflected from the high impedance front end of this machine. While the added inductance of the PRS load is a noticeable perturbation, on the whole, the energy dumped into the large (25 nH) initial front end inductance in the first 115 ns or so sets the amount of energy available in the load. Added to this rather stiff driver behavior is the common phenomenon of insulator stack flashover as the power flow reverses, which further decouples the load from the driver. Under such conditions the use of typical experimental voltage waveforms as boundary conditions to drive various load models can be expected to be reasonably accurate and is, in fact, effective in accounting for the experimental behavior.

A detailed accounting of the Phoenix line elements in Table I. shows the position of various monitors referred to in subsequent figures and in the typical experimental dataset. There are three common monitor stations extracted from the model as timeseries or waveforms --- the tube voltage (TV) , the tube current (TC), and the vacuum feed current (VFC). The location of each monitor within a given subset of line elements is shown, as well as the location of the flashover shunt (FS) at the insulator stack. In examining the probable effect of MITL losses near the PRS

loads the last four "constant gap MITL" positions are equipped with Child-Langmuir shunts dependent on local voltage for their resistance and generalized to include the effect of magnetic insulation on the electron and ion currents.

Table I. Phoenix Line Elements

Line Component	Number of 0.1 ns Elements	Impedance [Ω]	Inductance [nH]	Monitor Point
Tube Voltage Monitor	1	.56	0.056	TV
Water Flare A	20	0.55	1.10	·
Water Flare B	10	1.10	1.10	·
Water Flare C	25	1.15	2.87	·
Water Flare D	10	1.68	1.68	TC [no.10]
Plastic	1	10.8	0.108	F S
Vacuum Flare A	2	12.15	2.43	·
Vacuum Flare B	2	10.15	2.03	·
Vacuum Flare C	3	3.15	0.945	·
Const Z MITL	9	2.0	1.80	VFC [no.5]
Const Gap MITL no.1	1	2.09	⇓	summed
Const Gap MITL no.2	1	2.37	·	·
Const Gap MITL no.3	1	2.82	·	·
Const Gap MITL no.4	1	3.48	·	·
Const Gap MITL no.5	1	4.57	·	·
Const Gap MITL no.6	1	6.69	·	·
Const Gap MITL no.7	1	8.12	21.1	inductance

The load impedance is determined as the (possibly time dependent) quotient

$$Z_{load} = \frac{Load\ Inductance}{Feed\ Time\ Delay}$$

as implied by the detailed load model. The feed time delay is just the transit time of a signal from the output point of the biconic MITL to the position of the initial current path in the load cavity. For a short circuit load, various combinations of the feed time delay and the series load resistance were used to get a best fit to the experimental behavior. With a fixed feed inductance of 4.639 [nH], the time delay was varied from 0.02 → .05 [ns] and the short resistance was varied from 0.15 → 0.25 [Ω]. For a PRS model the feed inductance is varied and the time delay held fixed, as a way of modeling the expansion or contraction of the MITL gap right near the load.

Short Circuit Loads

Just like any other pulser, a precise knowledge of the voltage in Phoenix is valuable because the voltage and current monitors in the water (TV and TC) serve to define the energy sent downstream to the load and thus establish the energy budget for any load or MITL loss processes, including the PRS radiation. Within the scope of this effort a true calibration using the Phoenix line model above has not been achieved, but a very reasonable self-consistency check has been done.

By studying a short circuit shot and driving the model with the measured voltage waveform, the current observed in the MITL can be compared to that predicted. Once the voltage peak value or load parameters are adjusted to meet the observed downstream current, the voltage on the monitor at peak current ($\dot{I}$=0) should coincide with the measured voltage value at that time, viz. there is no inductive correction involved. In short, if the line is modeled with sufficiently high precision, then both the time and magnitude of peak current should be predicted by setting load or peak voltage parameters. Unfortunately this tidy scenario is only true if (i) no phase shifts are introduced in the model relative to the experiment, and (ii) the load impedance and time delay are known to high precision. In the tested line configuration neither of these conditions are true.

The model peak current occurs about 10 ns too early and, because the peak current occurs near the zero point of the driver voltage, this small phase shift produces a large relative uncertainty in the "voltage at peak current". All attempts to alter this phase shift by changing the short circuit load parameters (inductance, time delay, and resistance) show that only the peak current value changes. The time of peak current remains the same, to within the resolution of the calculation. The small phase shift is therefore likely coming from some divergence in particular model line parameters with respect to the experiment.

The line behavior also shows that the fit to peak current magnitude is not unique on the space of short circuit load parameters. In particular, the present study constrained:

[i.] the inductance to that typical of the PRS front end feed arrangement (4.639 nH),

[ii.] the resistance to a range compatible with the observed energy dissipation in the short circuit loads (≈0.1 Ω), and

[iii.] the feed time delay to a range compatible with the physical dimensions of the feed (≈0.05 ns).

In Table II. are shown the combinations of feed time delay and series load resistance which were tried and the peak current which resulted. Taking the voltage monitor signal at face value, these cases were all run at a fixed value for the peak driver voltage --- the observed value of 2.079 MV.

Table II. Peak Current Variations with Shorted Load Parameters

Short Circuit	Shunt [Ω]	⇒			
⇓Delay [ns]	0.15	0.175	0.200	0.225	0.250
0.020					
0.025	4.308 MA	4.216 MA	3.952 MA		
0.030		4.325 MA	4.222 MA	4.121 MA	4.023 MA
0.050			4.501 MA		

The observed peak current for the shot (# 705) was ≈4.0 MA, so the experiment can be matched by a variety of load parameters. In the best fit case above (0.030, 0.250) the observed absorbed energy in the shorted front end peaked at 380 kJ, while the model computed 414 kJ. The line current and voltage history of a calculation mimicing shot # 705 are shown in Figure 1 as surface plots. Since the line model elements are all at a constant 0.1ns, the line position grid spreads at the water -- vacuum interface. The flashover at the insulator is set to occur at a reversed polarity of 250 kV and shows as a flattening of the line voltage surface in Figure 1b. The tube and MITL currents diverge after this event, in consonance with experimental traces, and the MITL current downstream of the short shows (apart from some ringing) a weak "L/R" decay characteristic of the given front end inductance of about 25 nH and the inferred 0.25 Ω load resistor.

Clearly some further fine tuning could be done, but the general agreement is adequate unless further information is developed to constrain the shorted load

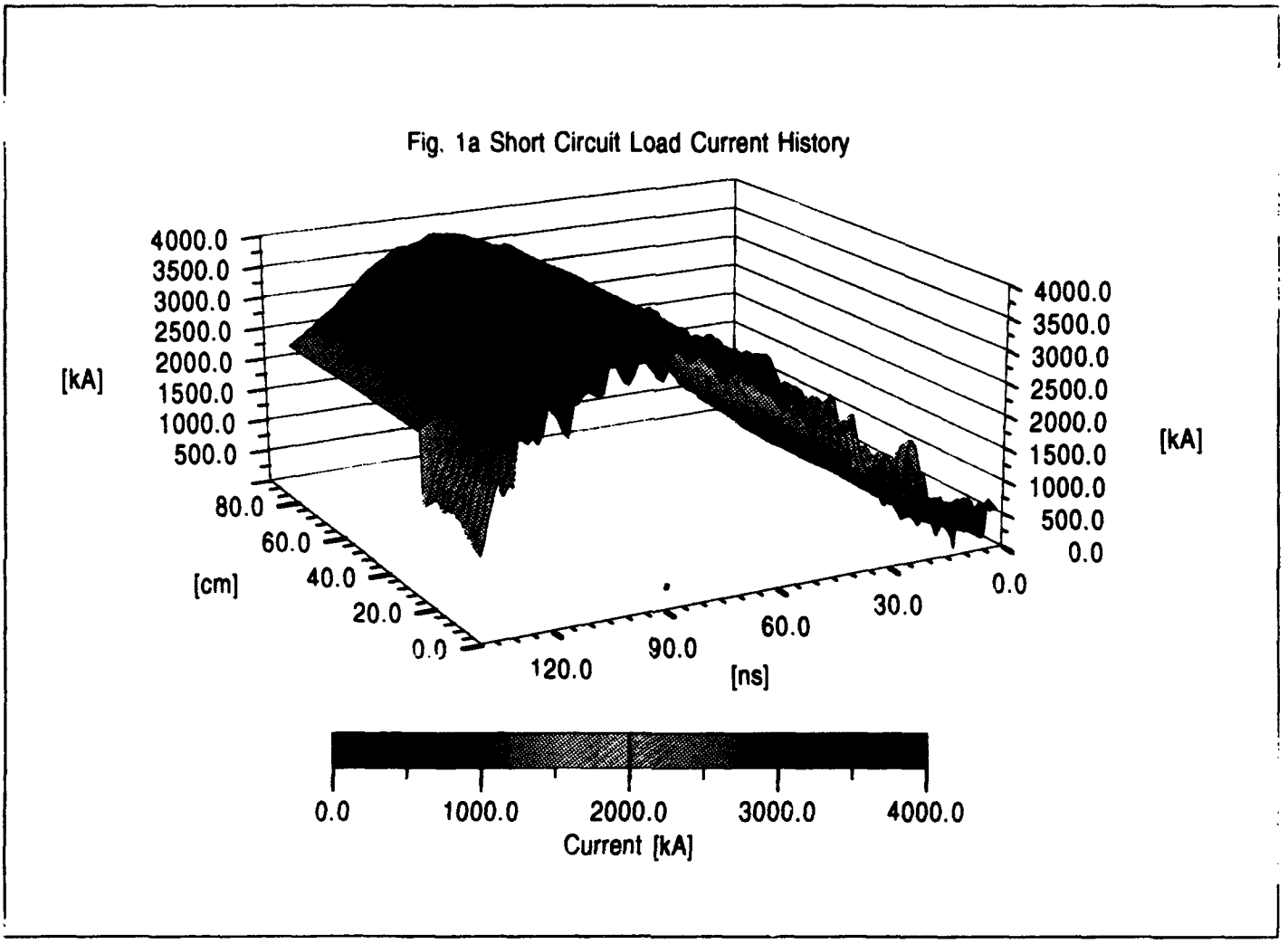

Fig. 1 — (a) Spacetime history of the line current in a shorted event. Spacetime history of the line voltage in a shorted event. The vacuum interface flashover site is indicated.

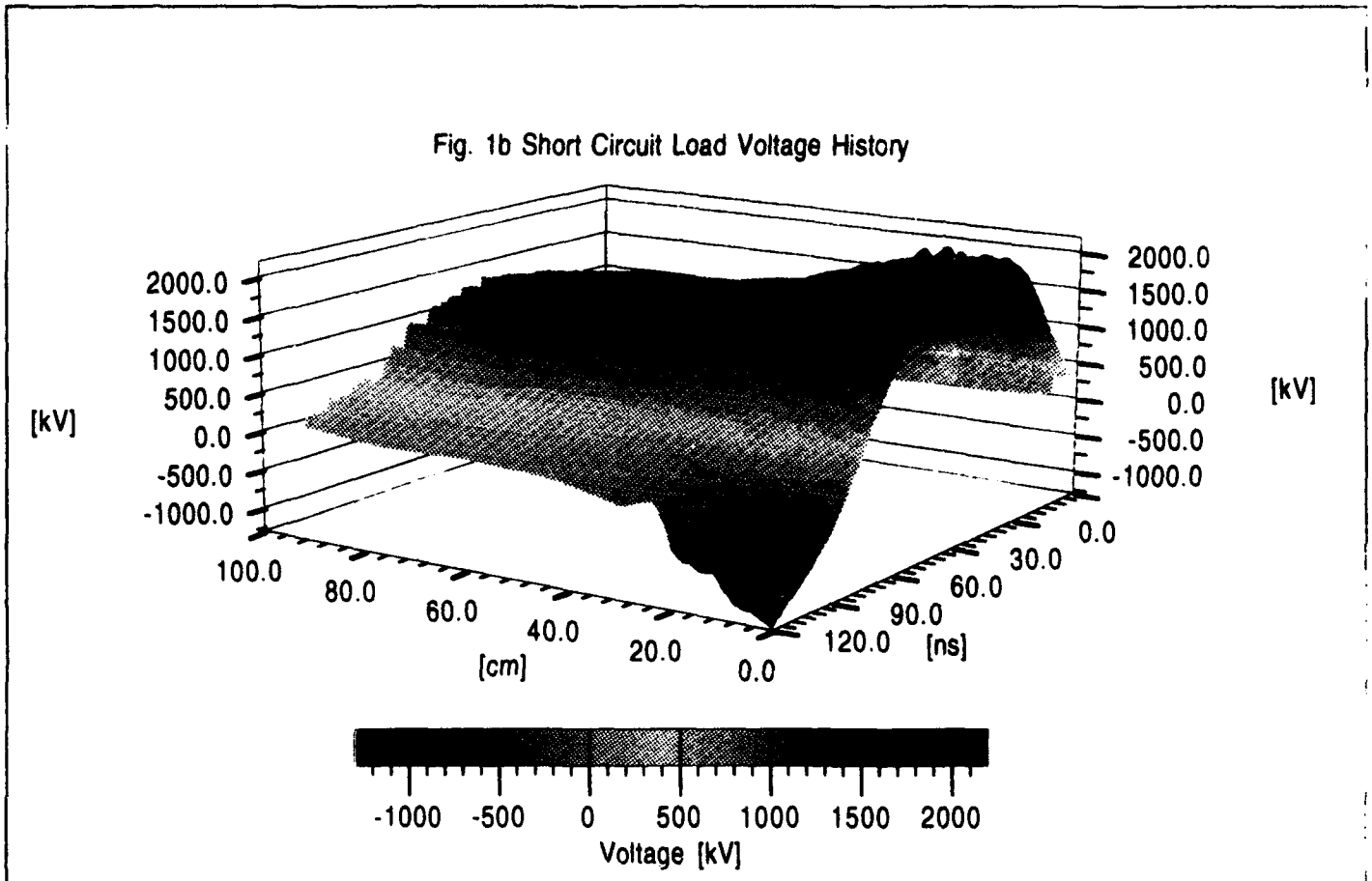

Fig. 1 — Continued (a) Spacetime history of the line current in a shorted event. Spacetime history of the line voltage in a shorted event. The vacuum interface flashover site is indicated.

parameters further. Unless the complete set of load parameters is known to high precision, it is equally clear that there is no basis for questioning or correcting the voltage calibration in the system.

Optimizing Kinetic Energy Delivery

Because of (i) the relatively high front end impedance of Phoenix, (ii) the fast risetime (of the voltage pulse typically measured at the TV monitor), and (iii) the insulator flashover event near the peak of reversed voltage, the energy coupling to a PRS may benefit from the insertion of as much energy as possible into the front end before flashover. If the flashover is early in the driver pulse these three considerations are even more important. Larger front end energy means larger inductance near the load, and this must sooner or later act to choke off the required current to the PRS. The tradeoff to be explored is then: how much inductance can be added, and where?

If the inductance is added to the feeds immediately around the PRS, then any loss of magnetic insulation near peak compression may be mitigated somewhat and allow more energy to drive the final moments of PRS stagnation. If the inductance is added to the load chamber by making the load longer, then more material is allowed to participate in the implosion, viz. each nH of added inductance produces a proportionate addition to the kJ of kinetic energy available to drive radiation.

In the present context these modifications can be simulated by changes in two load model parameters: the initial feed inductance and the load AK gap. The other relevant PRS variables: an initial load mass of 45 μgm/cm at an initial radius of 1.75 cm, imbedded in a return current structure of 2.0 cm radius, are kept fixed in the study. In addition the slug phase load resistance is kept at 0.25 Ω, since this value appears compatible with the short circuit data; while the minimum radius for the transition from annular to filled mode is set to 0.35 cm, since this value is compatible with the expected thickness of a gas puff load. Any radically smaller value for the slug phase resistance tends to produce too high a load current in the calculation to be compatible with the data. Such large apparent resistances may indicate a rather high level of turbulent or anomalous resistivity in the plasma phase of the loads, or

may indicate a disruption of the current path by the ablation of cold quasi-neutral material.

The calculation is also equipped with Child-Langmuir shunts in the MITL near the load feeds. As models for any anode and cathode plasmas which might arise later in the voltage pulse, these shunts allow ion current losses (H) or bipolar losses should a failure of magnetic insulation occur. Model behavior indicates that they will indeed "turn on" late in the implosion after stagnation when the plasma flow reverses in the computation and causes a strong power reflection. Experimentally however the observed feed currents tend not to show any strong rebound after the PRS stagnates and it is quite possible that the load doesn't recoil strongly at all in this machine. If the load model were made to mimic such a soft implosion, then the MITL shunts would probably not draw any significant current. The typical PRS implosion behavior is shown in Figures 2 and 3. The variables in Figure 2. are normalized to the values given in the legend and are defined as follows:

E_{load}, the energy accumulated in the load cavity,

E_{line}, the energy accumulated in the line (plotted negatively),

V_{load}, the voltage inferred at the PRS feed,

I_{mon}, the MITL current (plotted negatively) at the point VFC (Table I.),

V_{tube}, the voltage at the point VT (Table I.), and

I_{tube}, the waterline current (plotted negatively) at the point TC (Table I.).

The variables in Figure 3. are normalized to the values given in the legend and are defined as follows:

R, the load radius through the stagnation process, after the annular phase ends,

KE, the kinetic energy accumulated in the plasma flow (plotted negatively),

L, the inductance inferred at the PRS feed as the load collapses,

E_{ind}, the energy accumulated in that inductance (plotted negatively), and

Q_{int}, the total internal energy accumulated in the plasma load (plotted negatively).

It is from such diagnostics that the model predictions of peak kinetic energy, stagnation temperature, and transfer efficiency are derived. Note, in Figure 2, that

Fig. 2 Phoenix PRS Voltages and Currents [0—150ns].

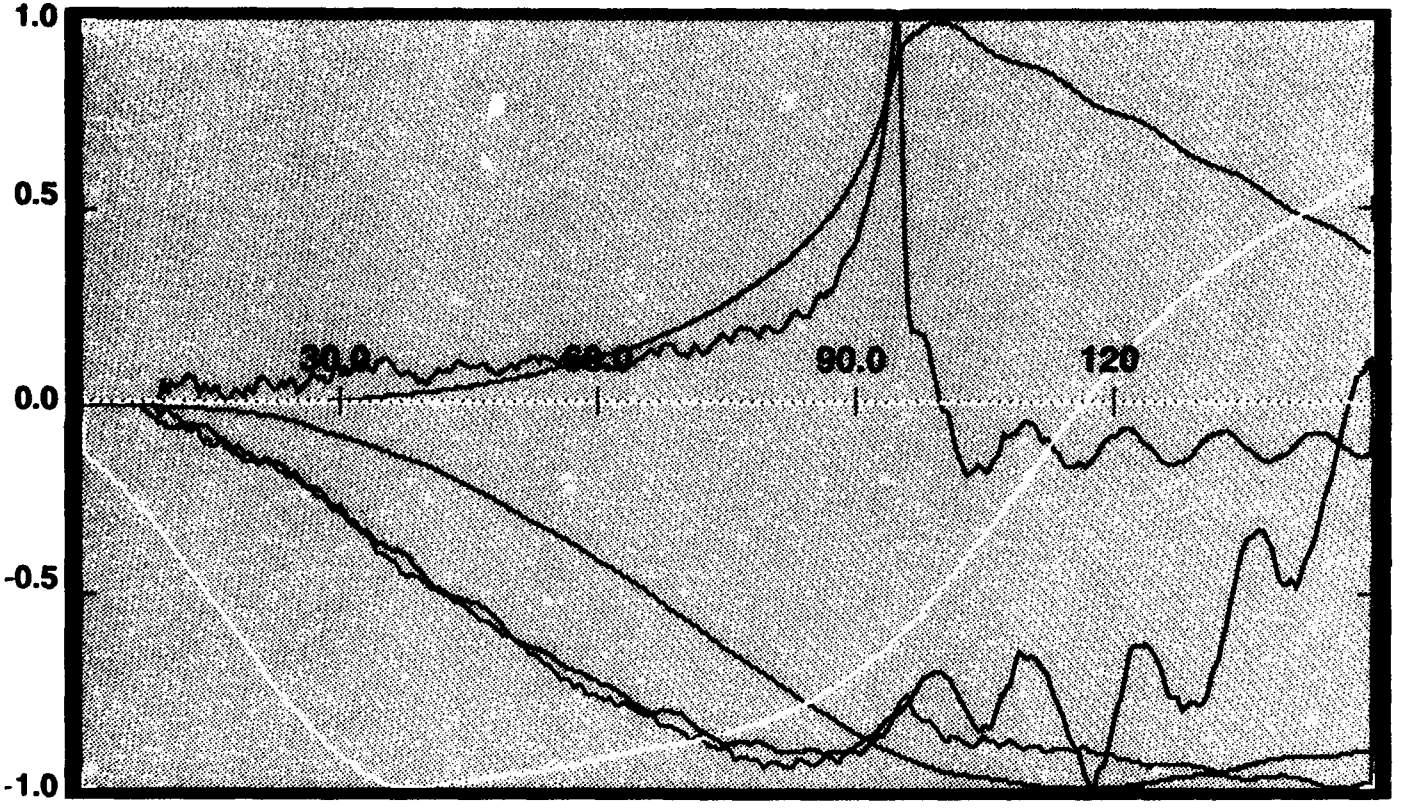

E_{load}[J]	E_{line}[J]	V_{load}[kV]	I_{mon}[kA]	V_{tube}[kV]	I_{tube}[kA]
2.56E005	7.41E005	6.25E003	5.43E003	2.83E003	5.65E003

..[A].. ..[B].. ..[C].. ..[D].. ..[F]..

Fig. 2 — Voltage and current traces (see text) typical of a PRS calculation with peak absolute values normalized as shown in the legend. Some quantities are plotted negatively to separate the curves.

Fig. 3 Phoenix PRS Load Variables [75—150 ns].

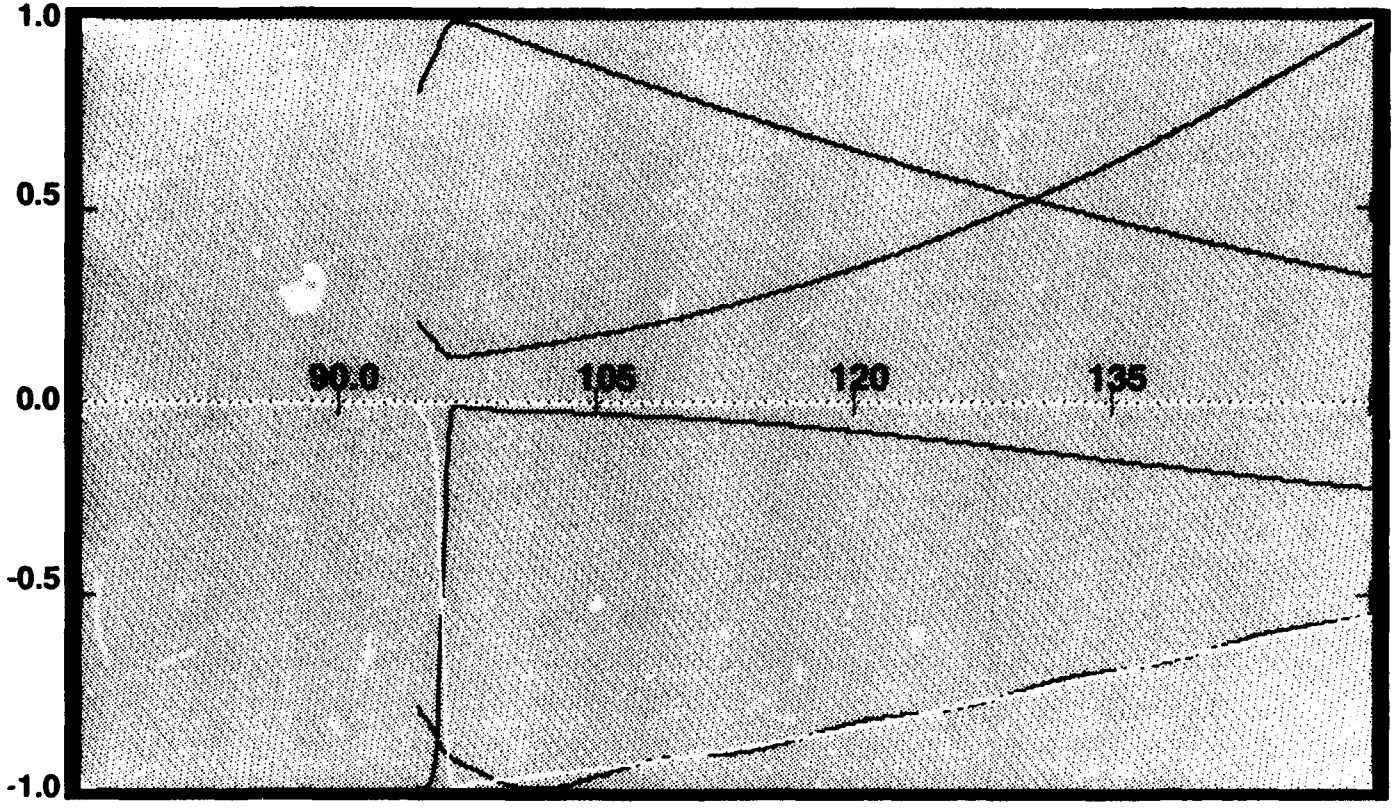

R[cm]	KE[kJ]	L[nH]	E_{ind}[kJ]	Q_{int}[kJ]
1.60E000	6.22E001	1.88E001	1.38E002	1.91E002
..[A]..	..[B]..	..[C]..	..[D]..	

Fig. 3 — Load energy and radial variations (see text) in a typical PRS calculation, with peak absolute values normalized as shown in the legend. Some quantities are plotted negatively to separate the curves.

the PRS model trips the flashover event at stagnation, as can be seen in the divergence of the tube current and monitor (MITL) current as the load voltage undergoes its reversal.

The variation of the peak load kinetic energy and the peak MITL current achieved in the implosion with feed inductance L_{feed} and gap size ℓ_{Load} is shown in the following tables and charts. The peak load kinetic energy [Table III.] is determined during the load stagnation process, viz. after the transition from an annular shell to a filled cylinder. The scaling of this kinetic energy with pinch length is generally sublinear, with short loads showing some periodic dips as the feed inductance changes. The undulation is probably due to unfavorable timing of reflections to the PRS for particular combinations of load and MITL inductance. When the load is longer the undulations die out because the variable load inductance is more significant relative to the inital feed inductance.

Table III. Peak Load Kinetic Energy Variations with Load Parameters

KE [kJ]			ℓ_{Load}		
L_{feed}	[cm] ⇒				
⇓ [nH]	3.0	3.5	4.0	4.5	5.0
4.65	50.0	71.7	78.7	86.0	92.1
4.80	49.4	70.9	77.9	85.1	91.2
4.95	62.5	70.2	77.1	84.3	90.4
5.10	61.5	69.5	76.3	83.5	89.6
5.25	48.0	68.8	75.6	82.7	88.7
5.40	47.4	68.1	74.9	81.9	87.9
5.55	59.6	67.4	74.2	81.2	87.1
5.70	59.0	66.8	73.5	80.5	86.4

The peak stagnation temperature, a measure of the specific kinetic energy imparted, is recorded at maximum compression [Fig. 4a]. A simple measure of overall machine transfer efficiency is just $\Theta_L \equiv \frac{E_{load}}{E_{line}}$, taking the ratio of the peak energy delivered to the load to the peak energy delivered to the MITL from the water line [Fig. 4b]. Increasing the pinch length improves the specific kinetic energy per ion until the pinch exceeds 4 cm; it also improves the transfer efficiency. Increasing the initial

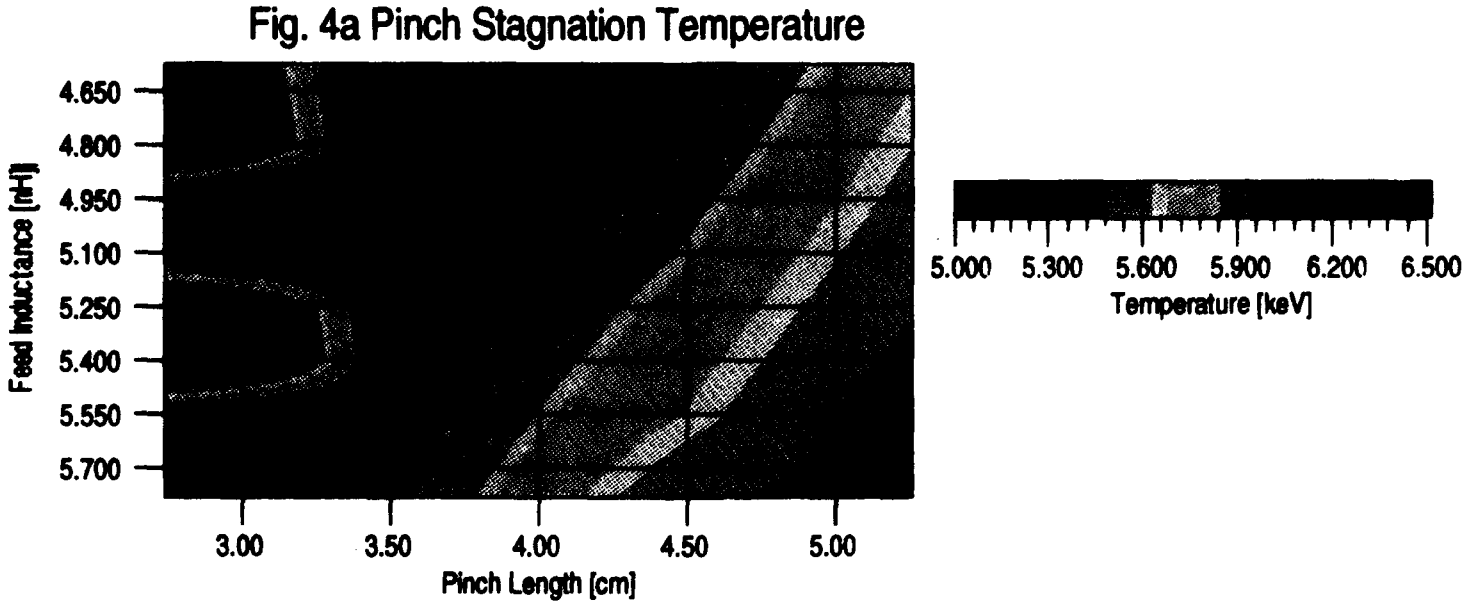

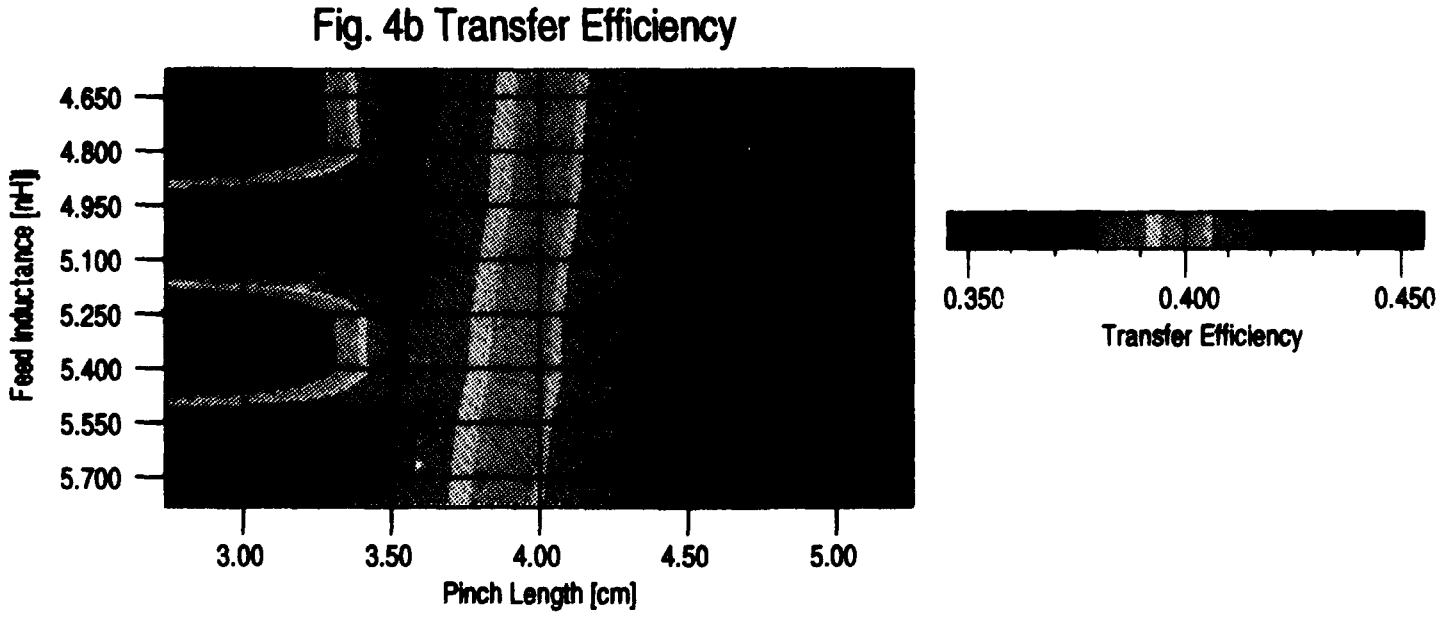

Fig. 4 — PRS performance summaries on the domain of feed inductance and load length in a 45 μgm/cm load: (a) peak stagnation temperature [keV], and (b) transfer efficiency.

feed inductance always drops the delivered kinetic energy, but raises the transfer efficiency slightly.

III. GAS PUFF NOZZLE

An assessment of the performance of Argon PRS sources on the pulse power machine Phoenix was made using a two-dimensional radiation-hydrodynamics code. The motivation for this work was to investigate nozzle designs which could optimize the uniformity of the implosion through high Mach number and tilting. Non-uniform implosions can greatly reduce the K-shell yield. Therefore, the primary objective of this set of simulations was to determine the optimum nozzle design for K-shell radiative output.

The computer code used to make these simulation was the 2-D radiation hydrodynamics code, PRISM, which was developed at NRL. The 2-D MHD code, PRISM, has been used in a variety of problems dealing with Z-pinches. For instance, comparison of experiments and simulations of implosions on the 6 TW Double-Eagle generator at Physics International were found to be in good agreement (C. Deeney, P. D. LePell, F. L. Cochran, M. C. Coulter, K. G. Whitney, and J. Davis, Phys. Fluids B 5, 1000(1993)). The simulations were able to predict the general trend of yield optimization with tilted nozzle angle. A factor of 4 increase in yield observed experimentally in the case of the best nozzle design was also predicted by the 2-D simulations.

In the simulations reported on here, an initialization module was used which specifies the density of the particular nozzle on the 2-D computational grid. A nearly flat density profile is chosen within the interior region of the nozzle gas, while the annular cross-section of the load is modeled as $e^{-(\frac{r-r_0}{r_s})^4}$ with r_0 a mounting radius and r_s a scale length. This profile was used in earlier simulations of gas puff implosions because it appeared to give a relatively good fit to experimental measurements. In any case, the actual functional form of the cross-section is not a sensitive parameter because of the strong compression of the gas (see Fig. 5) during the early stage of the implosion. The simulations were run in a Lagrangian remap mode in order to

3 cm DIAMETER NOZZLE - 0° TILT

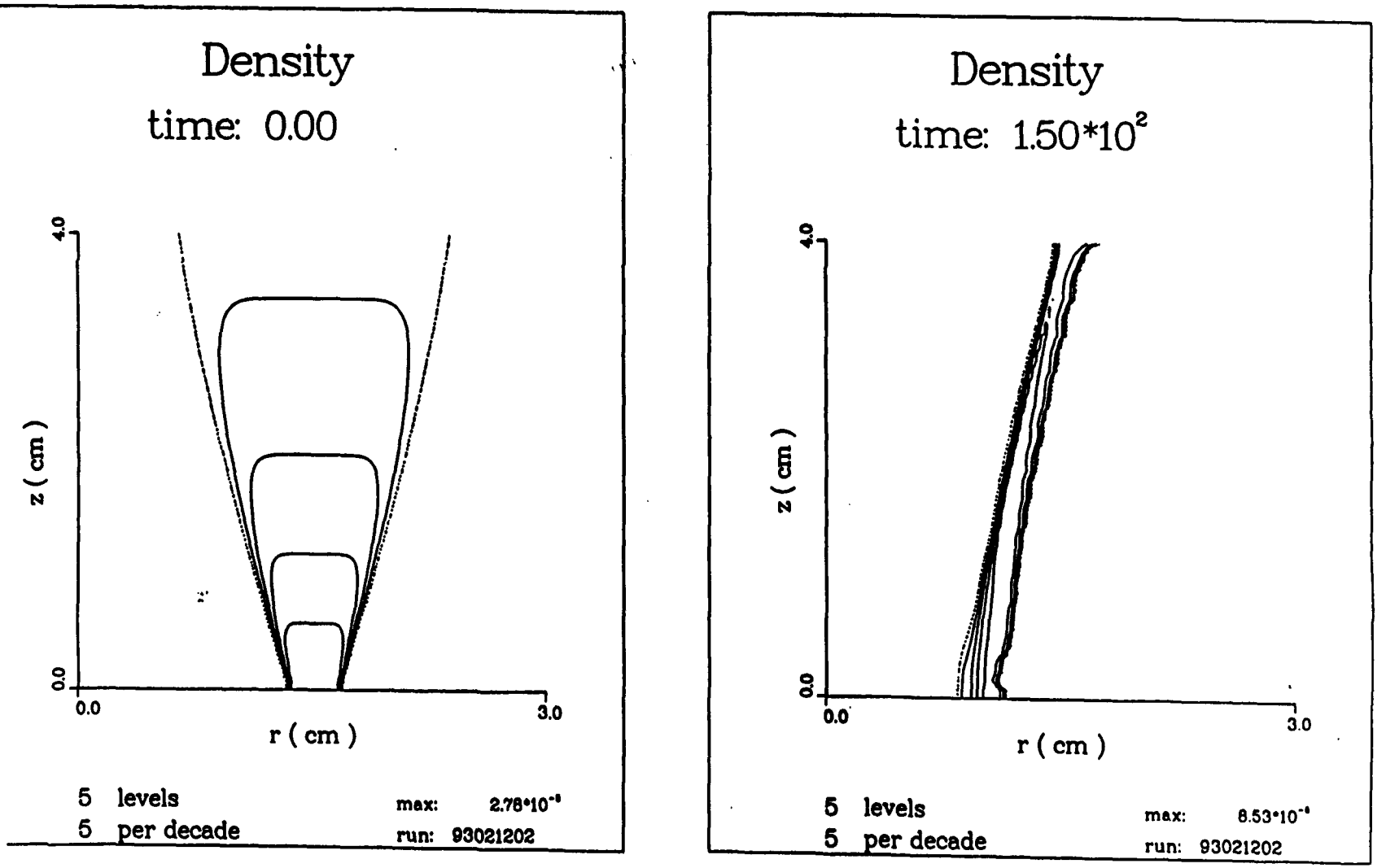

Fig. 5 — Density plots for the 3 cm diameter untilted nozzle at 0 and 150 nsec.

accommodate the large distortions of the gas during the runin. That is, the grid was continuously adjusted after each Lagrangian cycle so that it remained orthogonal in r and z. The radiative power was determined during each computational cycle through the use of lookup tables and a local opacity model. The radiated power term affects the dynamics of the pinch through its inclusion in the energy equation.

The tilted nozzle calculations reported on here were made with a lumped circuit equation for modeling the Phoenix current profile. Key parameters used were: a machine inductance of 18.5 nh and a resistance of 0.55 ohms. A voltage profile of the Phoenix generator was used as input. The return current diameter was set to 7.3 cm.

In all of the simulations, the above values were used in the circuit equation with initial plasma diameters of 3 cm, 3.7 cm, and 3.4 cm (i.e., diameters measured at the center of the nozzle aperture). The diode length was set to 4 cm. All of these radii had the same initial mass of 100 μgm/cm of Argon. In addition, the initial nozzle design consisted of a 3 mm output aperture and a flow rate set to a value of Mach 5. Such an optimistic (high Mach number) design implies that the initial puff will form a thin shell with minimal expansion along the z-axis. It is more likely that the expansion from an actual gas puff nozzle will result in a Mach number of about 3 due to turbulence and boundary layer effects. Lower Mach number nozzles are discussed further later in this report.

Figures 5 and 6 show density contours during the implosion of an untilted, 3 cm diameter nozzle (the gas flow Mach number and mass are as given above). The maximum value of the density (given in gm/cm^3) and the contour level structure are shown at the bottom of each figure (e.g., 5 levels with 5 per decade means that this is a log plot with five contours spanning from the maximum density to 0.1 of the maximum density). The time values are in nsec starting from the beginning of the simulation. Zippering, a phenomena characteristic of uneven implosions, is evident in Figure 6. At the final time in Fig. 6, density contours are shown near the time of maximum radiative power. The density can be seen to be concentrated in a single high density region along the axis. After this time, the dense region continues to

3 cm DIAMETER NOZZLE - 0° TILT

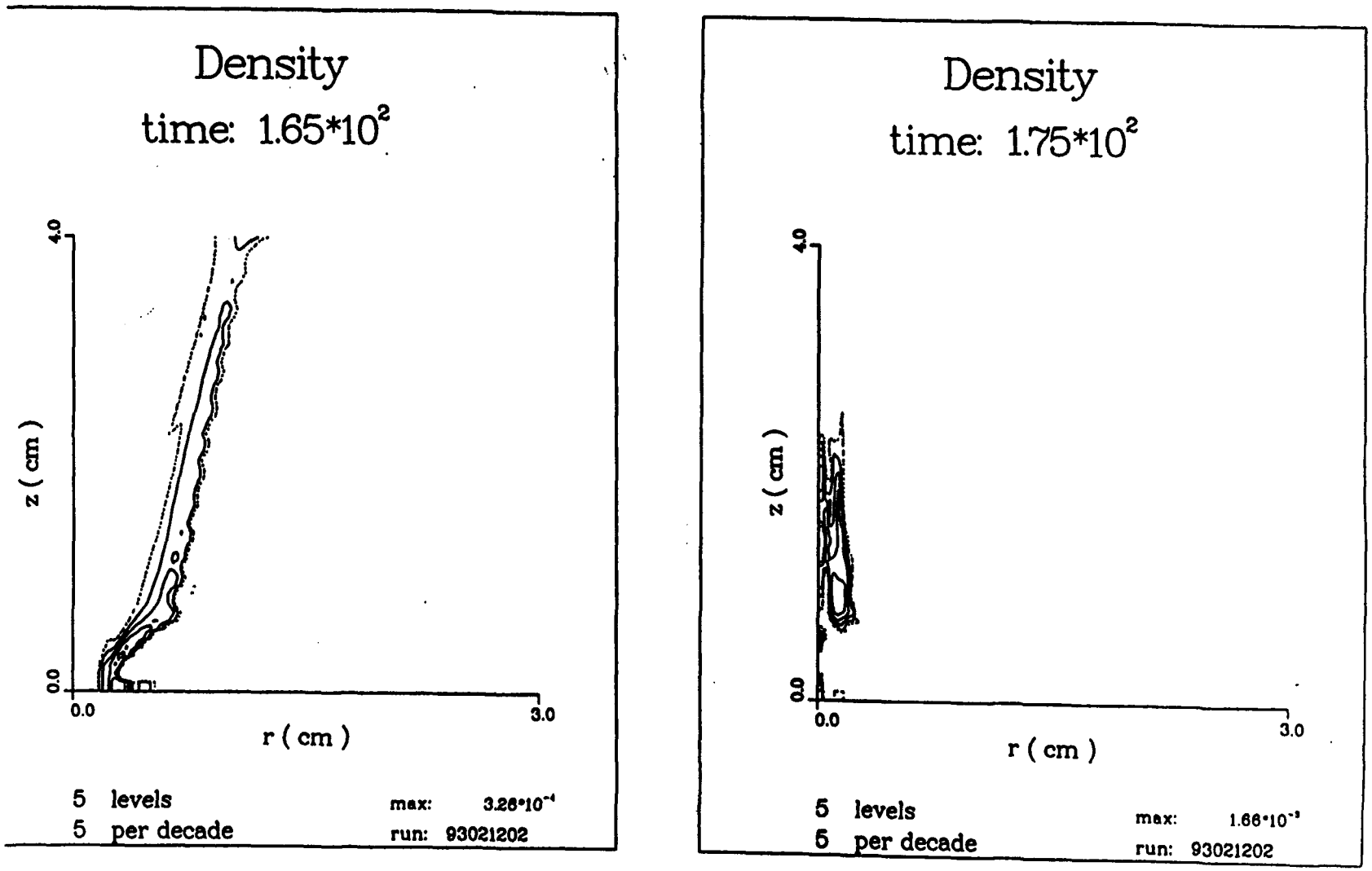

Fig. 6 — Density plots for the 3 cm diameter untilted nozzle at 165 and 175 nsec.

move up the axis. The result is that a relatively wide, low power, K-shell radiation pulse is produced.

In Figures 7 and 8, the results of a simulation are shown in which a 7.5° inward tilt is added to the nozzle. The tilt is employed in an attempt to reduce the zippering by counteracting the gas expansion as it moves away from the nozzle exit. During the final phase of the implosion some structure can be seen but dense regions are evident along the entire central axis. Moreover, these regions stagnate on axis nearly simultaneously. This produces a high power and narrow width radiation pulse. In addition, since there is little of the jetting action which accompanies a zippered implosion and limits the on-axis density, the peak density values in the compressed regions can be much larger than the density in a non-tilted implosion. This results in larger yields as well as higher peak powers because the radiative power is dependent on the density as well as the total number of radiators.

The instantaneous K-shell power density for the 0° and 7.5° tilted nozzles are shown in Figure 9. The distribution along the axis of the radiating regions in the tilted case and the localized region in the untilted case closely resembles the density contour plots. The much higher maximum power density achieved with the tilted nozzle is also evident.

Figures 10 and 11 show the time history of the current and the spatially integrated K-shell power for the two cases discussed above. Peak current in both cases is about 3.5 - 4.0 MA and the implosion takes place between 170-180 nsec. The narrow, high power pulse which results from the tilted nozzle implosion can be clearly seen in Fig. 9. The spatially integrated peak K-shell power is nearly an order of magnitude larger in the tilted case versus the untilted case. The FWHM (i.e., Full Width at Half-Maximum) of the K-shell power is also considerably less than in the untilted case.

The current and radiation pulses for the 3.7 cm diameter nozzle simulations with 0° and 7.5° tilt angles are shown in Figures 12 and 13 respectively. The same enhancement in the radiation power level for the tilted nozzle design is seen in this

3 cm DIAMETER NOZZLE −7.5° TILT

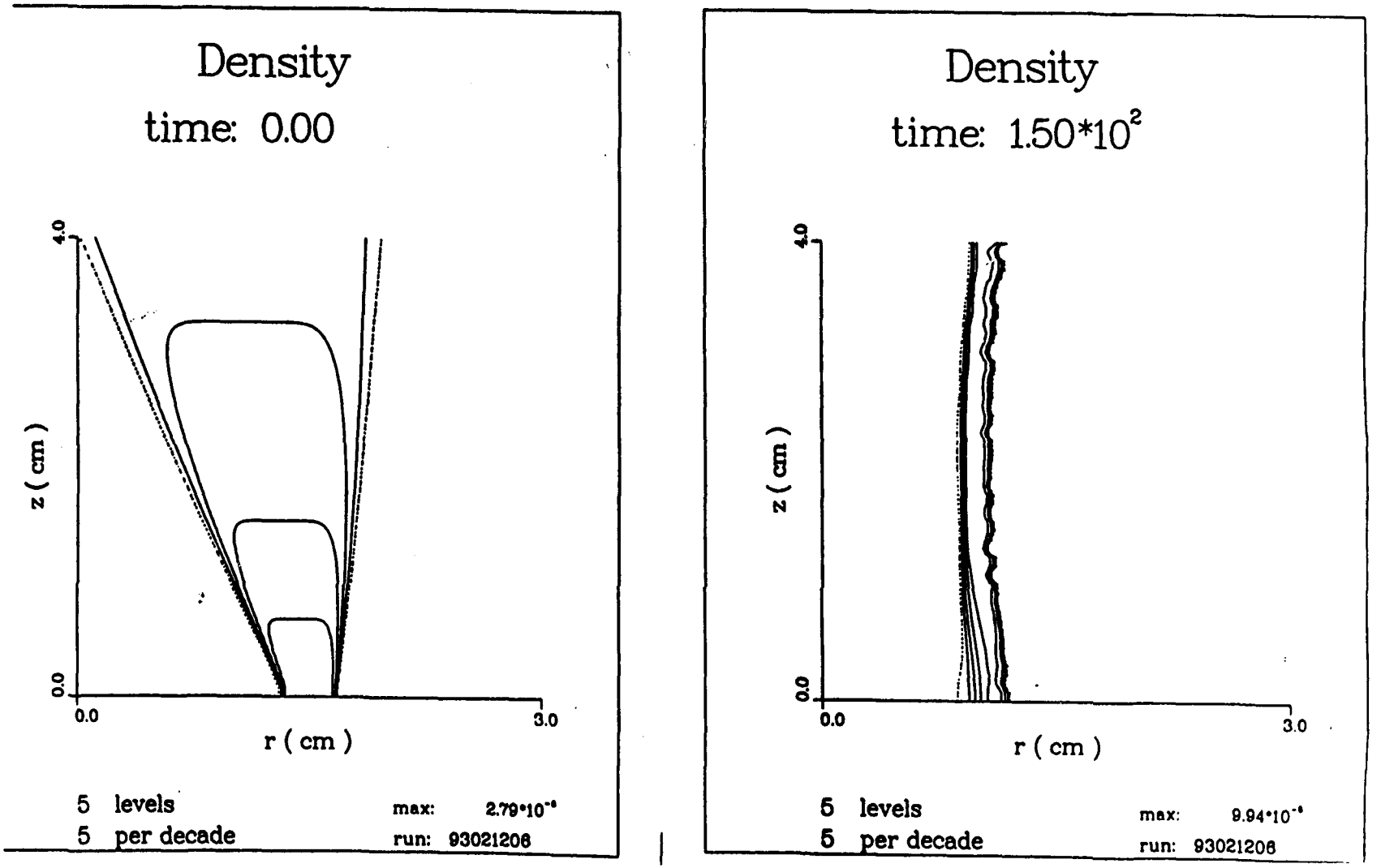

Fig. 7 — Density plots for the 3 cm diameter tilted nozzle (-7.5°) at 0 and 150 nsec.

3 cm DIAMETER NOZZLE −7.5° TILT

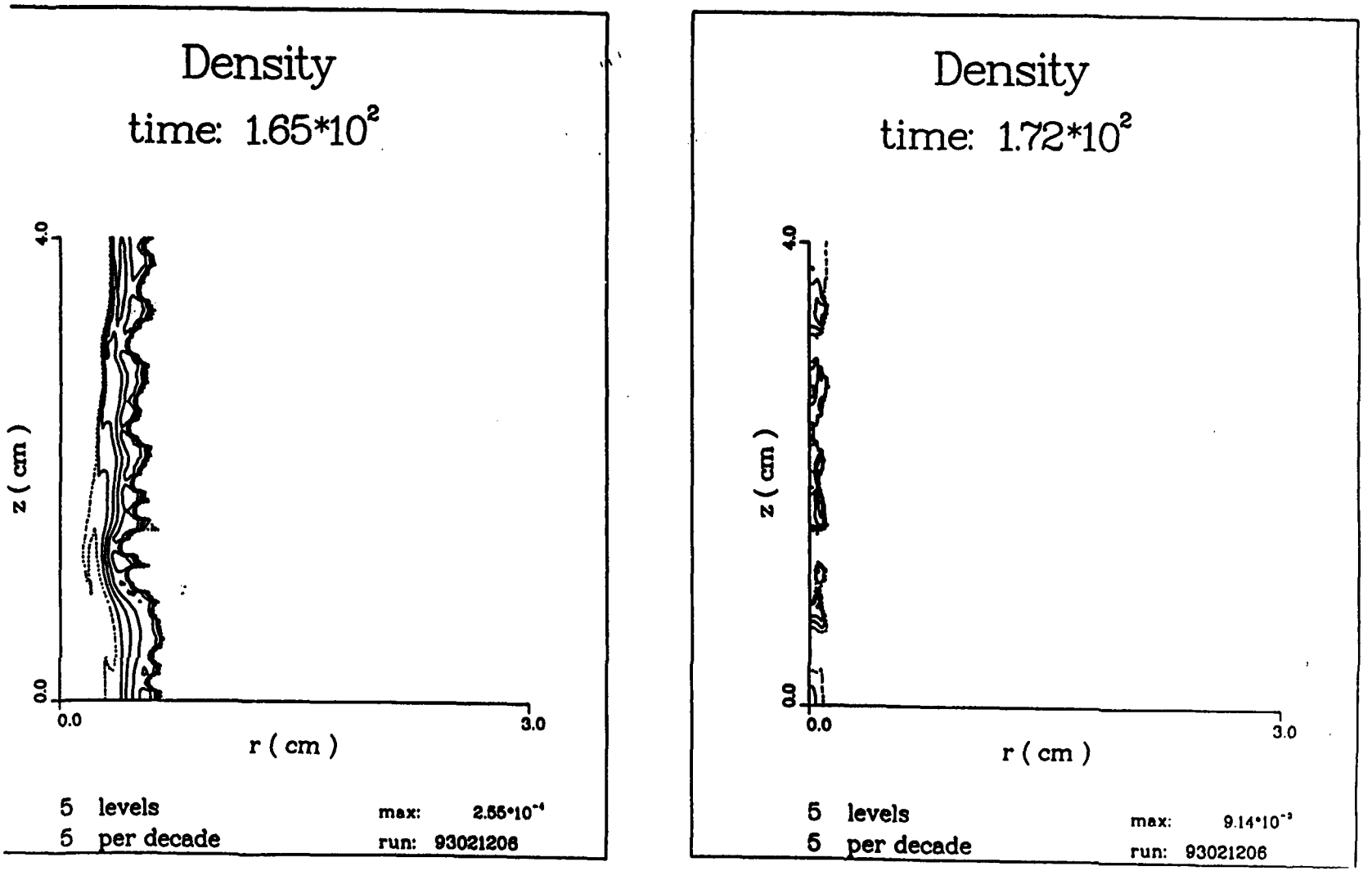

Fig. 8 — Density plots for the 3 cm diameter tilted nozzle (-7.5°) at 165 and 172 nsec.

3 cm DIAMETER NOZZLE - 0° TILT

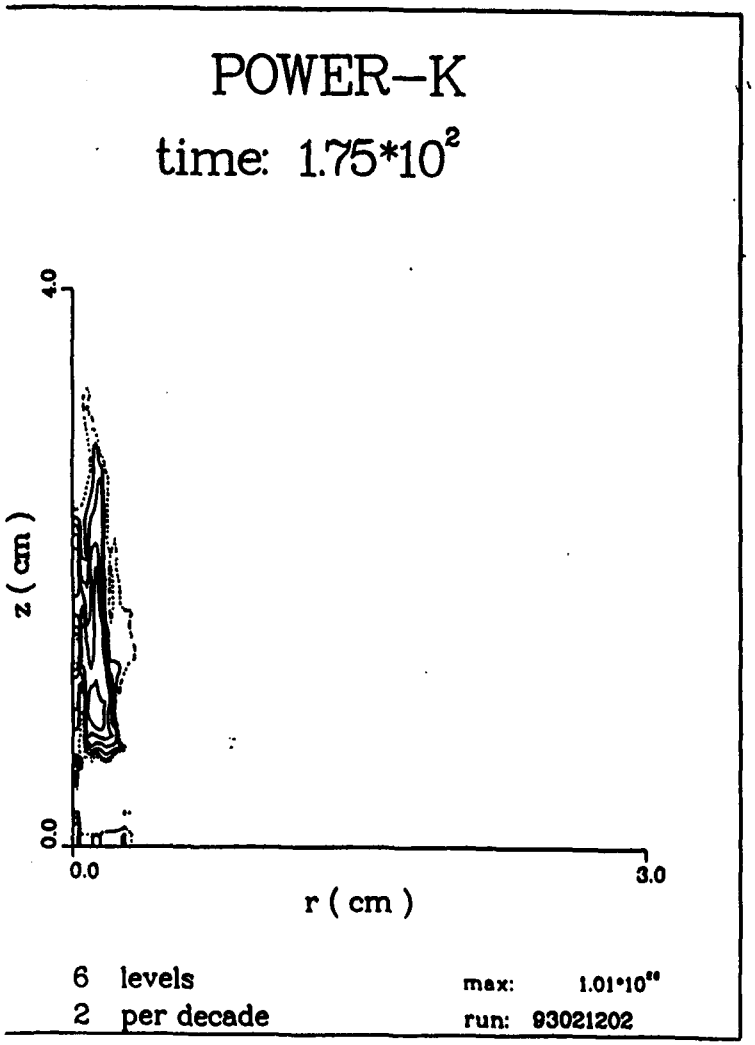

3 cm DIAMETER NOZZLE –7.5° TILT

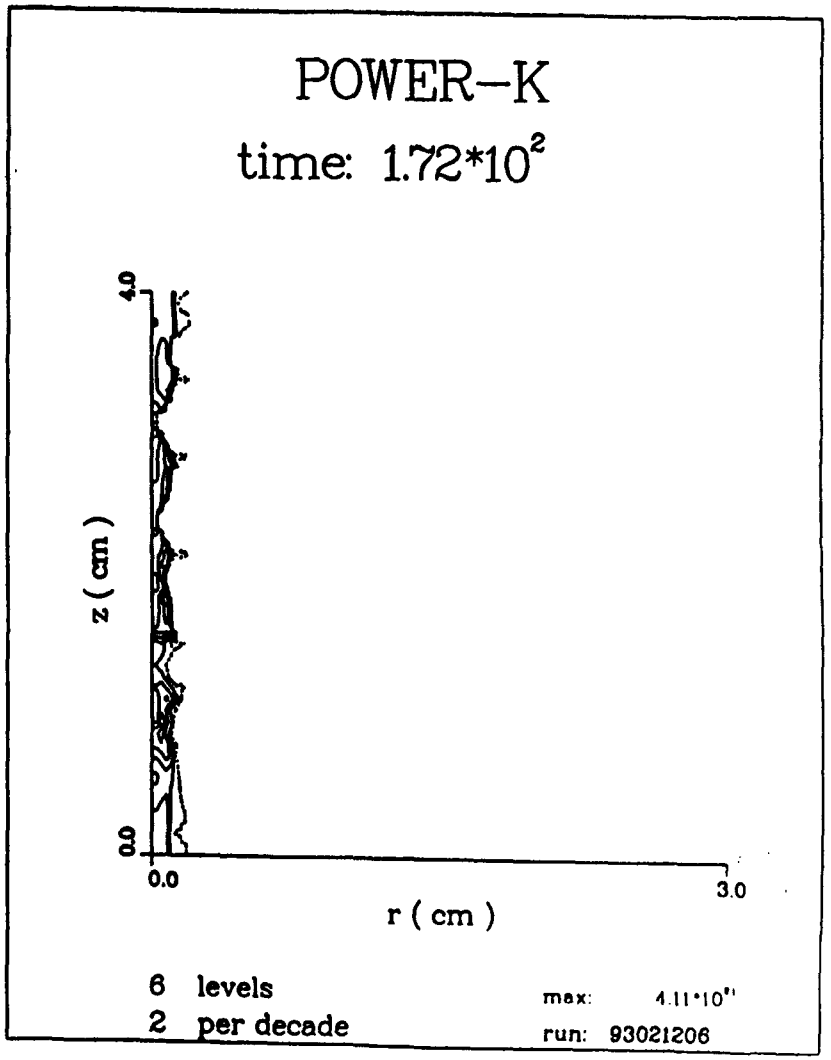

Fig. 9 — K-shell power near maximum compression on axis for the 3 cm diameter untilted and tilted nozzles.

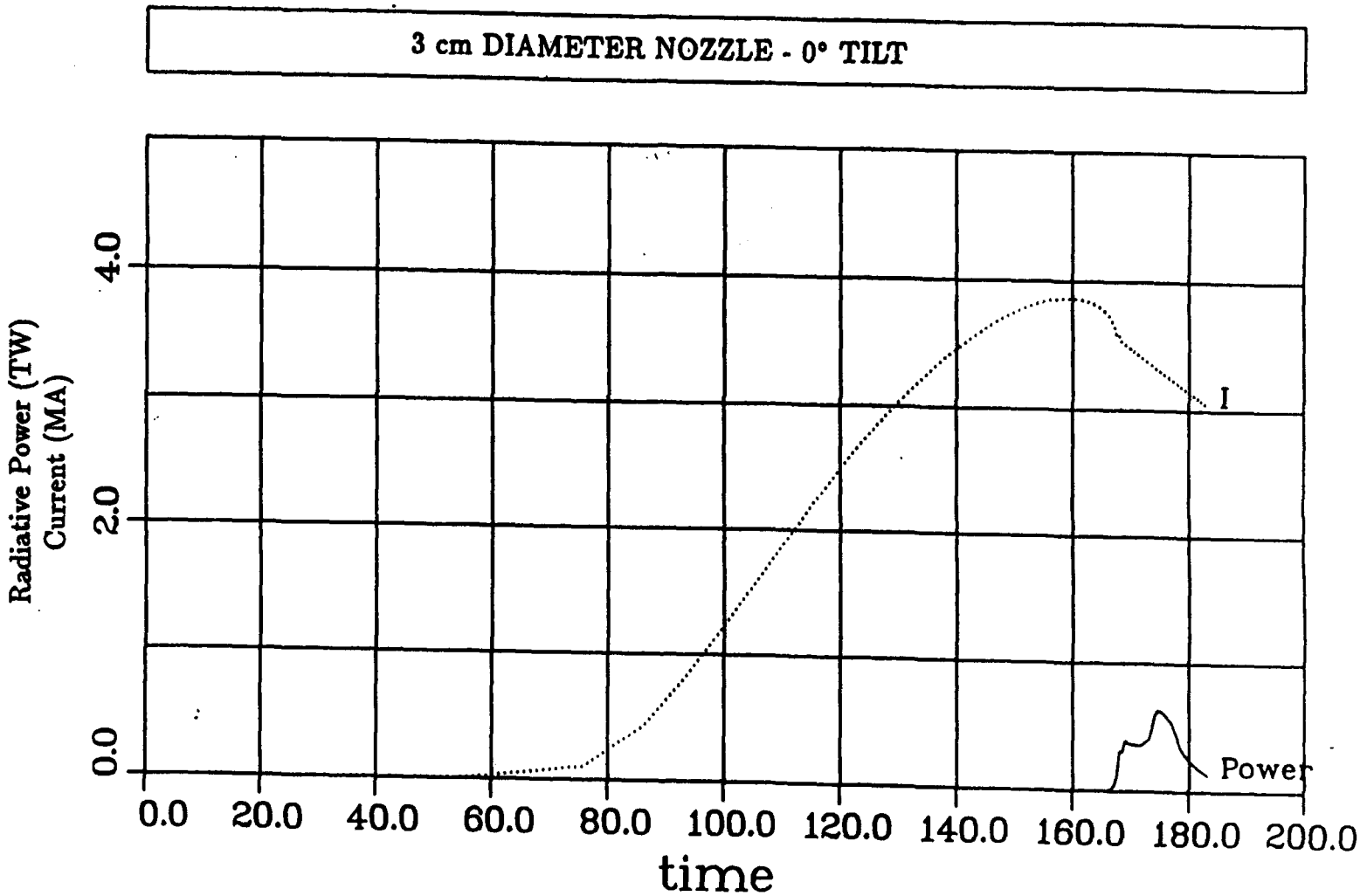

Fig. 10 — Time histories of the load current and K-shell radiative power for the 3 cm diameter untilted nozzle simulation.

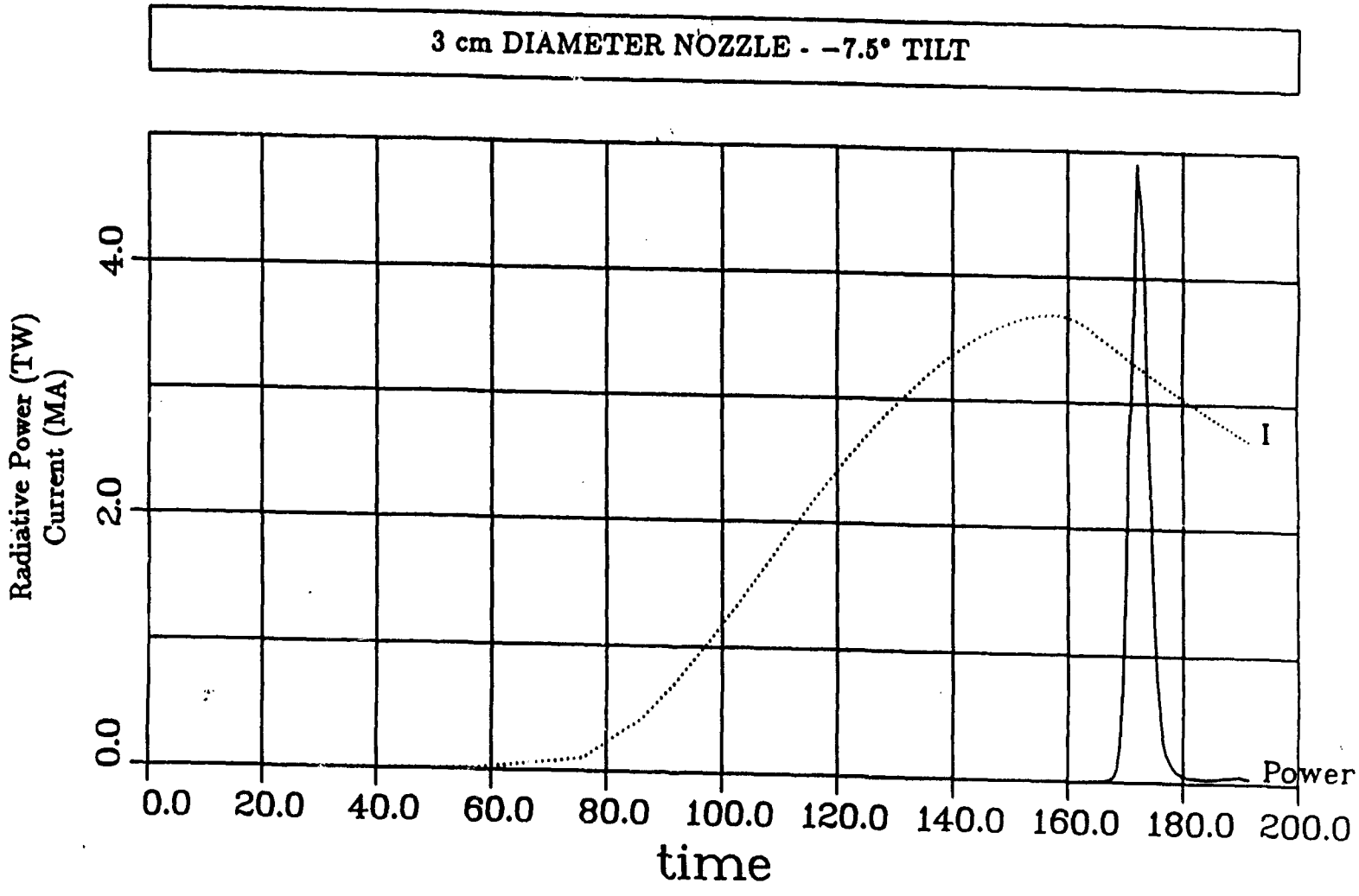

Fig. 11 — Time histories for the 3 cm diameter tilted nozzle simulation.

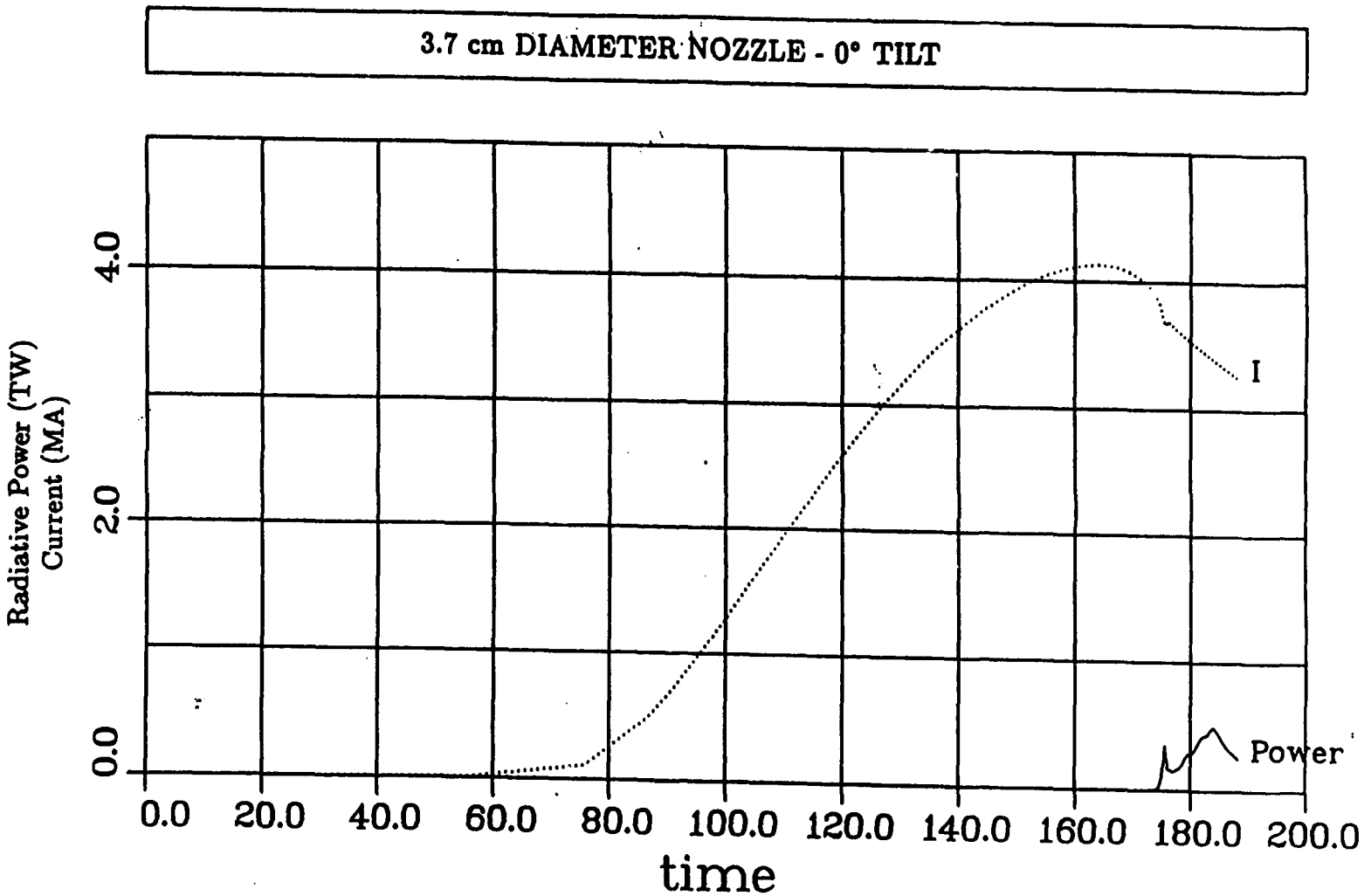

Fig. 12 — Time histories for the 3.7 cm diameter untilted nozzle simulation.

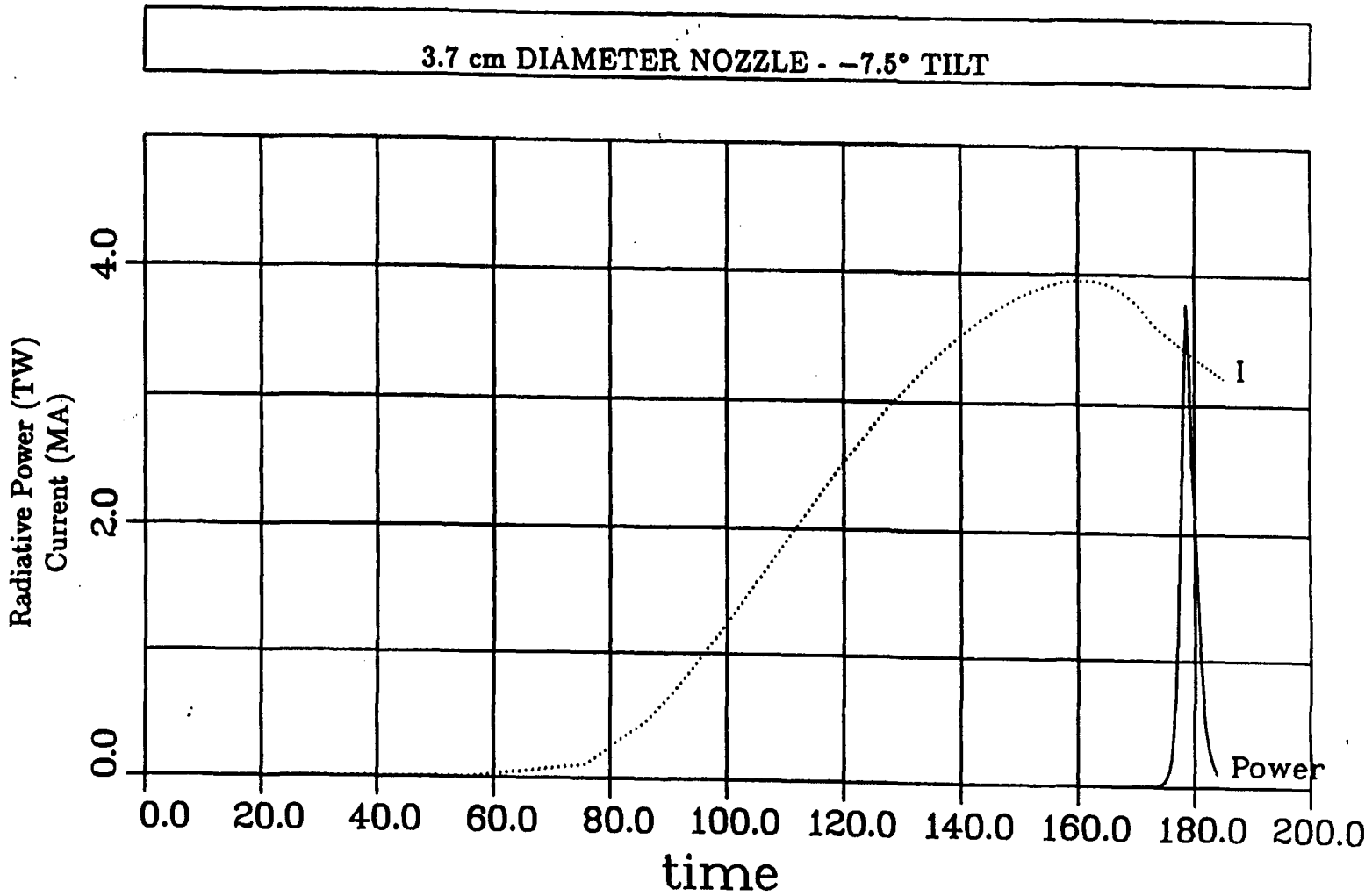

Fig. 13 — Time histories for the 3.7 cm diameter tilted nozzle simulation (-7.5°).

case. It should also be noted that the longer runin time allows the peak current to go slightly above 4 MA in the untilted case and to nearly 4 MA in the tilted case. This makes it apparent that in a high density, uniform implosion the inductive effects of a tighter pinch result in a slightly lower peak current.

Figures 14 and 15 show the radiation pulse and current for the 4.5 cm diameter nozzles. The longer runin again results in higher peak currents as is the case with the 3.7 cm nozzles.

The results for three nozzle diameters, (3 cm, 3.7 cm, and 4.5 cm) each with four inward tilt angles (0°, 5°, 7.5°, and 10°) are summarized in Figure 16. The highest K-shell yield for a Mach 5 nozzle is slightly above 20 kJ (100 μgm/cm, 3 cm diameter nozzle). For all diameter nozzles, the peak in the K-shell power appears to take place at a 7.5° inward tilt angle.

This process was repeated for two more Mach number nozzles: Mach 3 and Mach 4. These Mach numbers are more likely to be closer to the value which will actually be realized in an experiment because of boundary layer effects and turbulence. The results from a series of simulations are presented in Figure 17. It can be seen that at lower Mach numbers, the peak in the yield curve shifts to higher tilt angles in order to compensate for the increased expansion of the gas exiting the nozzle. At a Mach number of 3, the tilt angle must be increased to 12° in order to counteract the gas expansion. However, the peak radiated yield is only marginally different for the three different Mach number nozzles. The explanation for this lies in the snowplow effect. It is important that the greatest amount of inwardly directed kinetic energy be coupled to the largest fraction of the initial mass. If a large amount of the mass is swept up before the implosion while there is still time to couple in kinetic energy, then the initial width of the puff will be of relatively little importance. If, however, the puff is so broad that only a small fraction of the mass couples to most of the kinetic energy before implosion, then the width of the gas profile will be of greater significance. The peak yield in all cases represents the optimized situation where the tilt of the nozzle best compensates for the radial expansion.

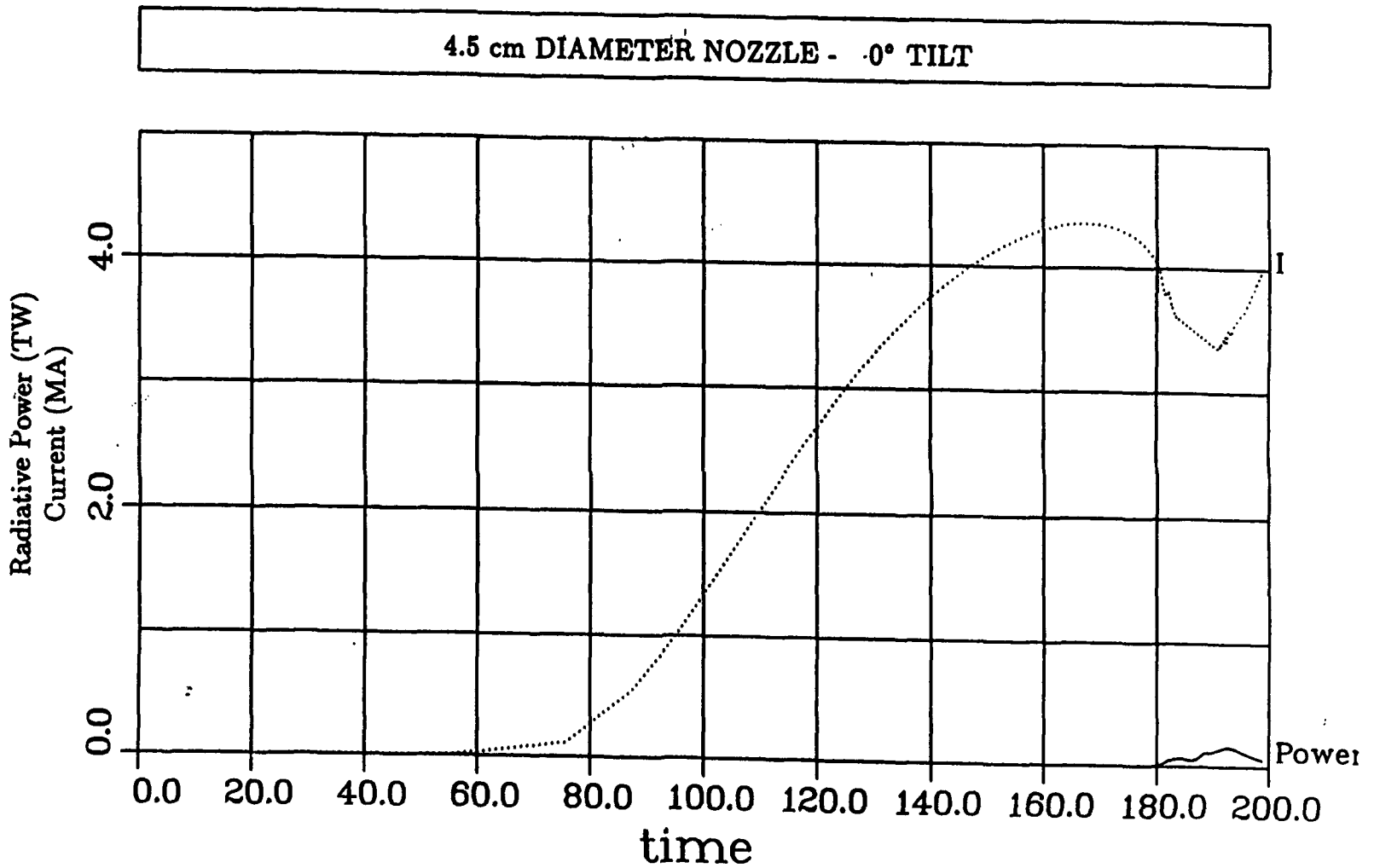

Fig. 14 — Time histories for the 4.5 cm diameter untilted nozzle simulation.

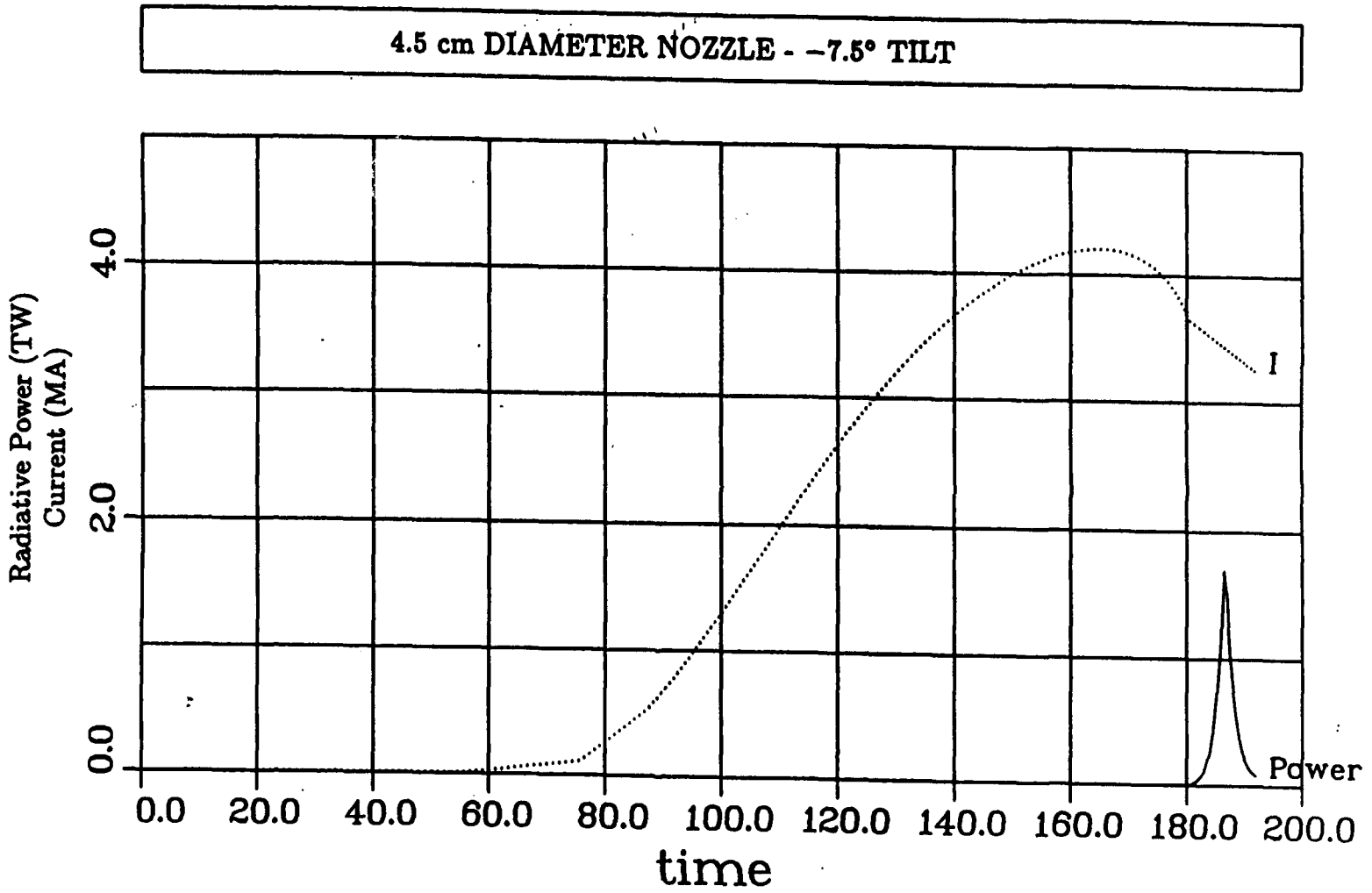

Fig. 15 — Time histories for the 4.5 cm diameter tilted nozzle simulation (-7.5°).

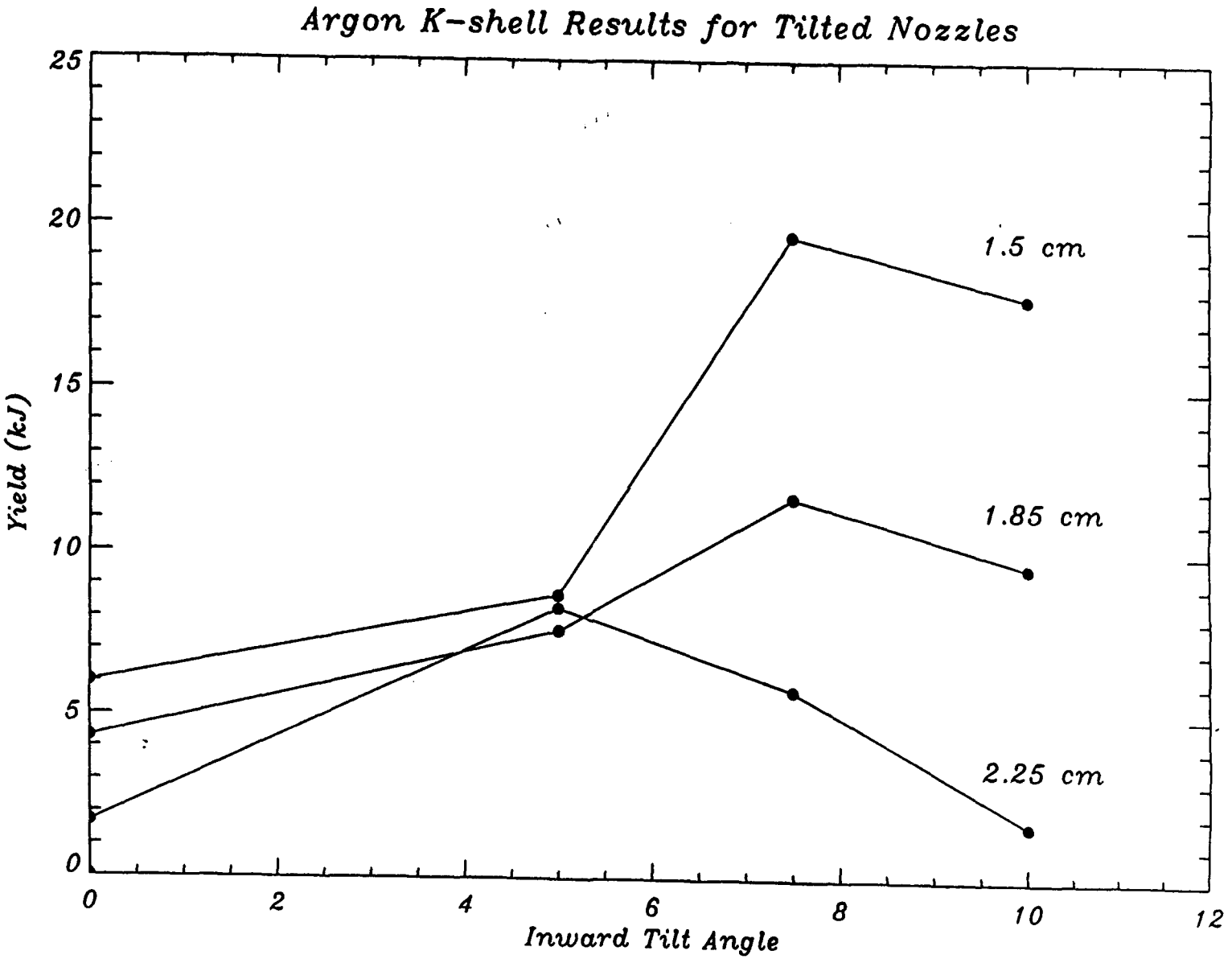

Fig. 16 — Argon K-shell yields as a function of tilt angle for the 3 different radii nozzles.

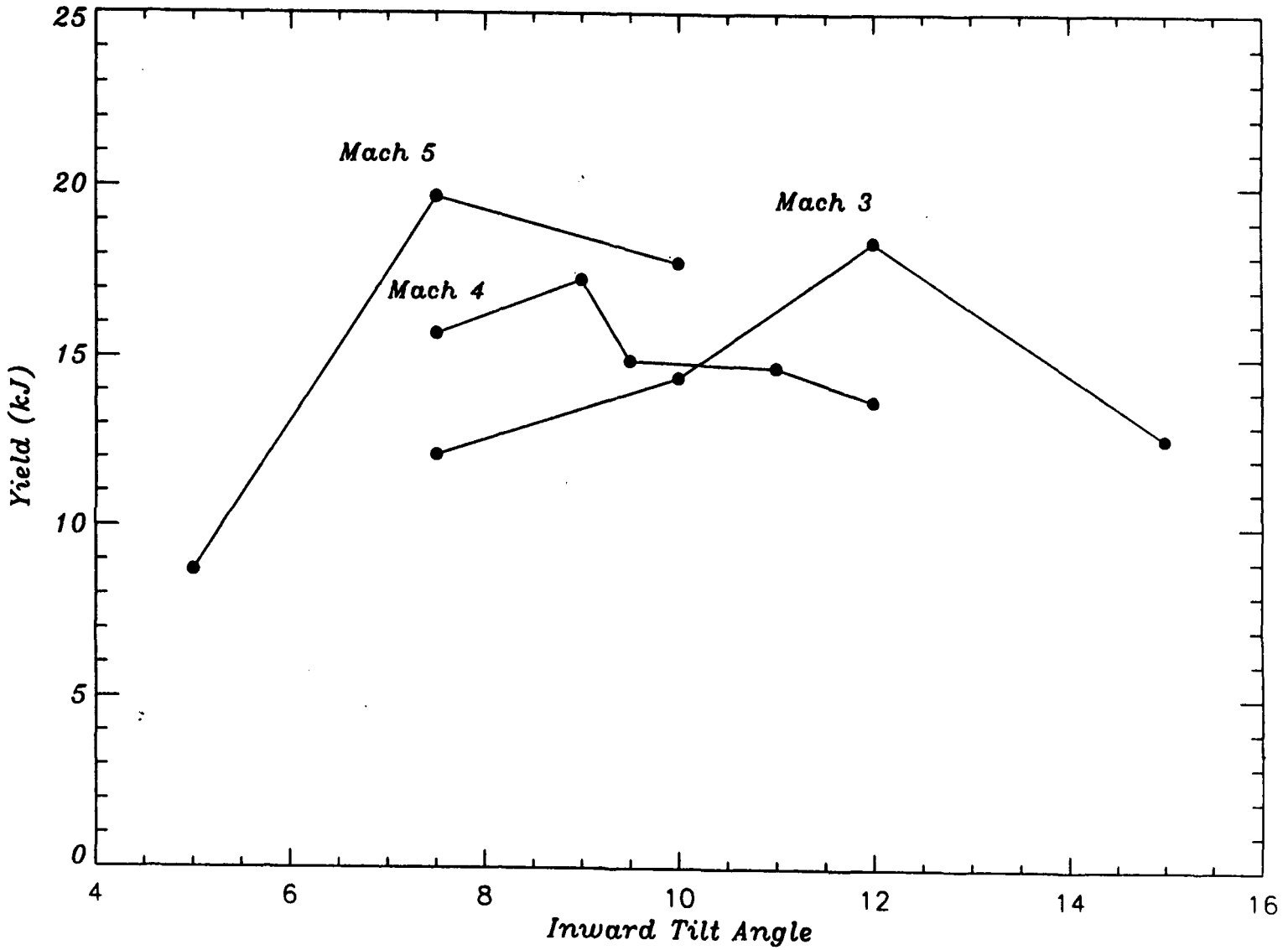

Fig. 17 — Argon K-shell yields as a function of tilt angle for three different Mach number nozzles (1.5 cm radius or 3.0 cm diameter nozzle).

IV. CONCLUSION

The foregoing analysis of the Phoenix pulser has provided a basic accounting of its operation as a PRS driver in three areas of interest. First, the basic calibration of the power flow has been shown to be self consistent, and the detailed requirements for obtaining a more precise check on the voltage monitor have been specified. Second, the kinetic energy delivery to a PRS load has been examined with respect to the feed inductance and load length. The agreement with experiment is generally quite good with respect to peak current, and the inferred kinetic energy. The modest optimizations of kinetic energy with feed inductance for the shorter load lengths should be checked experimentally, and a more detailed modeling study could follow. Third, the tilt angle of the gas puff nozzle has been shown to be very important in radiative yield optimization. The use of lower Mach number nozzles is probable in the actual lab situation, so the guidance developed here should play a role in the design and optimization.

Several areas could be researched further if the optimum PRS performance on Phoenix is to be realized. With regard to general power flow, the use of a matched, or nearly so, resistive load would provide the best opportunity to really achieve an in situ calibration of the power monitors. More detailed magnetic insulation theory, diagnostics, and simulation would provide a definitive answer to the questions of power loss in the feeds near the PRS. A general effort to design a front end geometry allowing a longer rundown distance for the gas puff PRS would also be a good path to follow.

Acknowledgements

The authors are grateful for the help of E. Nolting, V. Kenyon, L. Miles, W. Spicer, and J. Draper in characterizing the Phoenix machine and providing timely data.